# Viscoelastic properties of dynamically asymmetric binary fluids under shear flow

Vinay Dwivedi,[1,2] Rajeev Ahluwalia,[2] Turab Lookman,[2] and Avadh Saxena[2]
[1]*Department of Mechanical and Environmental Engineering, University of California, Santa Barbara, California 93106, USA*
[2]*Theoretical Division, Los Alamos National Laboratory, Los Alamos, New Mexico 87545, USA*
(Received 9 October 2003; revised manuscript received 16 April 2004; published 30 July 2004)

We study theoretically the viscoelastic properties of sheared binary fluids that have strong dynamical asymmetry between the two components. The dynamical asymmetry arises due to asymmetry between the viscoelastic stresses, particularly the bulk stress. Our calculations are based on the two-fluid model that incorporates the asymmetric stress distribution. We simulate the phase separation process under an externally imposed shear and compare the asymmetric case with the usual phase separation under shear flow without viscoelastic effects. We also simulate the behavior of phase-separated stable morphologies under applied shear and compute the stress relaxation.

DOI: 10.1103/PhysRevE.70.011506 PACS number(s): 83.50.Ax, 83.60.Bc, 64.75.+g

## I. INTRODUCTION

Many fluids can exhibit viscoelastic behavior; i.e., their response to deformation is intermediate between that of solids and fluids. For short times, the response is elastic and the stress is proportional to the applied strain. On the other hand, in the long-time limit, a fluidlike response with stress proportional to the strain rate is observed. The effect of viscoelasticity on the morphologies of phase separating polymer solutions and blends has been recently studied experimentally by Tanaka [1,2]. It is now well established that due to an asymmetry between the viscoelastic properties of the two phases, a transient network of the more viscoelastic phase is observed. While there is some understanding of the influence of viscoelastic effects on phase separation, little is known about how viscoelasticity affects phase separation when an external shear flow is applied. Although the effects of shear on Newtonian (purely hydrodynamic) binary fluids have been well studied [3,4] and dynamical steady states with stringy morphologies have been observed, it is also important to study similar situations for binary fluids where viscoelastic effects can dominate.

Theoretically, the coupling between the stress and concentration fluctuations was investigated by Helfand and Fredrickson [5] in the context of shear flow in polymer solutions. Doi and Onuki [6] studied this coupling by introducing a two-fluid model that considers two different velocities for the two components. Taniguchi and Onuki [7] have used the two-fluid model to study viscoelastic phase separation. However, a two-fluid model incorporating dynamical asymmetry due to the asymmetric distribution of bulk stresses [8–11] has successfully explained many features of the viscoelastic phase separation experiments of Tanaka [1,2], such as transient network formation and eventual phase inversion. Recently, this theory has also been applied to study the viscoelastic phase separation in diblock copolymers [12]. The two-fluid model was also used to simulate polymeric foams under shear [13]. In this paper, we use this model to study phase separation under shear flow for a binary fluid that is characterized by a strong asymmetry between the viscoelastic moduli of the two phases, particularly the bulk modulus.

In addition to phase separation under shear flow, a study of the behavior of the stable phase-separated states under deformation is also important. Recently, Buxton and Balazs [14] have studied the mechanical properties of phase-separated morphologies using a block and spring model. This model considers elastic properties but cannot describe the viscoelastic response. Thus we study the behavior of fully phase-separated stable states under a constant shear based on the two-fluid model. The time evolution of mechanical stresses generated for such phase-separated states is also studied.

The paper is organized as follows. In Sec. II, we discuss the two-fluid model used in our simulations. Section III describes results of viscoelastic phase separation under shear flow while Sec. IV is devoted to the response of stable phase-separated morphologies subjected to steady shear. We conclude the paper with a summary and discussion in Sec. V.

## II. TWO-FLUID MODEL

The coupling between viscoelastic stresses and diffusion is studied using the two-fluid model. We consider a dynamically asymmetric mixture of a viscoelastic fluid ($A$) and a purely hydrodynamic (nonviscoelastic) fluid ($B$). In this model, different velocity fields—$\vec{v}_A(\vec{r},t)$ for the viscoelastic phase and $\vec{v}_B(\vec{r},t)$ for the nonviscoelastic fluid—are introduced. The average velocity is given by $\vec{v}_{average}(\vec{r},t) = \phi(\vec{r},t)\vec{v}_A(\vec{r},t) + [1-\phi(\vec{r},t)]\vec{v}_B(\vec{r},t)$, where $\phi(\vec{r},t)$ is the concentration of the viscoelastic fluid. The free energy of mixing can be written in terms of the concentration $\phi(\vec{r},t)$ as

$$F_{mix} = \int d\vec{r}\,[\phi^2(1-\phi)^2 + (C/2)(\vec{\nabla}\phi)^2], \tag{1}$$

where $C$ is the concentration gradient coefficient that is assumed to be constant in the present work. The free energy $F_{mix}$ is a simplified version of the Flory-Huggins [15] free energy. The applied shear flow is implemented by considering an average velocity $\vec{v}_{average}=\vec{v}_{applied}+\vec{v}$, where $\vec{v}$ is the contribution to the average velocity due to concentration fluctuations and $\vec{v}_{applied}$ is the contribution due to the external shear flow given as

 

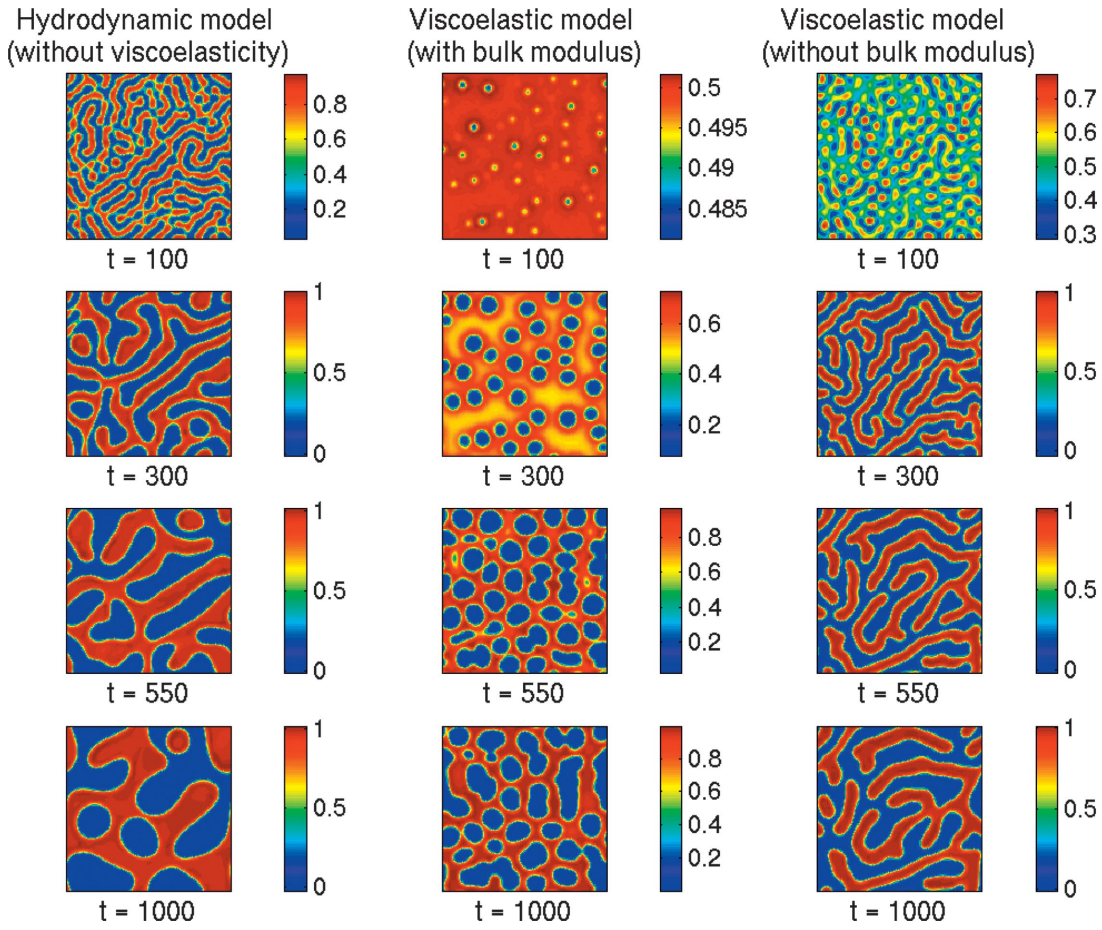


FIG. 1. (Color online) Phase separation process without shear flow for the purely hydrodynamic case, the viscoelastic case with bulk modulus, and the viscoelastic case without bulk modulus.

$$\vec{v}_{applied} = s|x - x_0|\hat{j}. \tag{2}$$

This represents an external shear (symmetric about $x_0$) applied along the $y$ direction and $s$ is the shear rate. The appropriate equation of motion for incompressible viscoelastic binary fluids under external shear flow is

$$\frac{\partial \phi}{\partial t} + \vec{v}\cdot\vec{\nabla}\phi + s|x - x_0|\frac{\partial \phi}{\partial y} = \vec{\nabla}\cdot\frac{\phi(1-\phi)^2}{\zeta}[\vec{\nabla}\cdot\overleftrightarrow{\Pi} - \vec{\nabla}\cdot\overleftrightarrow{\sigma}]. \tag{3}$$

Here $\overleftrightarrow{\sigma}$ represents the viscoelastic stress tensor. The osmotic tensor $\overleftrightarrow{\Pi}$ is defined as $\vec{\nabla}\cdot\overleftrightarrow{\Pi} = \phi\vec{\nabla}\{2\phi(1-\phi)^2 - 2(1-\phi)\phi^2 - C\nabla^2\phi\}$. The quantity $\zeta$ is the friction coefficient associated with the velocity $\vec{v}_A - \vec{v}_B$ and $\eta_s$ is the shear viscosity. The dynamics of the average velocity field $\vec{v}$ is given by the usual Navier-Stokes equation

$$\rho\frac{\partial \vec{v}}{\partial t} = -\vec{\nabla}\cdot\overleftrightarrow{\Pi} + \vec{\nabla}P + \vec{\nabla}\cdot\overleftrightarrow{\sigma} + \eta_s\nabla^2\vec{v}, \tag{4}$$

where a pressure has been introduced to account for the incompressibility constraint. If we use the overdamped limit $\partial\vec{v}/\partial t = 0$, then under the incompressibility condition $\vec{\nabla}\cdot\vec{v} = 0$, the velocity can be expressed in Fourier space as

$$\vec{v}_k = \overleftrightarrow{T}_k\cdot(-\vec{\nabla}\cdot\overleftrightarrow{\Pi} + \vec{\nabla}\cdot\overleftrightarrow{\sigma})_k, \tag{5}$$

where $(\cdots)_k$ represents the Fourier transform and $T_k$ is a tensor defined in Fourier space as

$$\overleftrightarrow{T}_k = \frac{1}{\eta_s k^2}\left[\overleftrightarrow{I} - \frac{\vec{k}\vec{k}}{k^2}\right], \tag{6}$$

where $\overleftrightarrow{I}$ represents the unit tensor. To specify a constitutive law for the viscoelastic stresses, we use the Maxwell model according to which the equation of motion for the stresses is given by

$$\frac{\partial\overleftrightarrow{\sigma}_b}{\partial t} + \frac{\overleftrightarrow{\sigma}_b}{\tau_b(\phi)} = m_b(\phi)\overleftrightarrow{M},$$

$$\frac{\partial\overleftrightarrow{\sigma}_s}{\partial t} + \frac{\overleftrightarrow{\sigma}_s}{\tau_s(\phi)} = m_s(\phi)\overleftrightarrow{M}, \tag{7}$$

where $\tau_b$ and $\tau_s$ are the internal molecular relaxation times associated with the bulk and shear stresses, respectively. The matrix $\overleftrightarrow{M}$ is given by

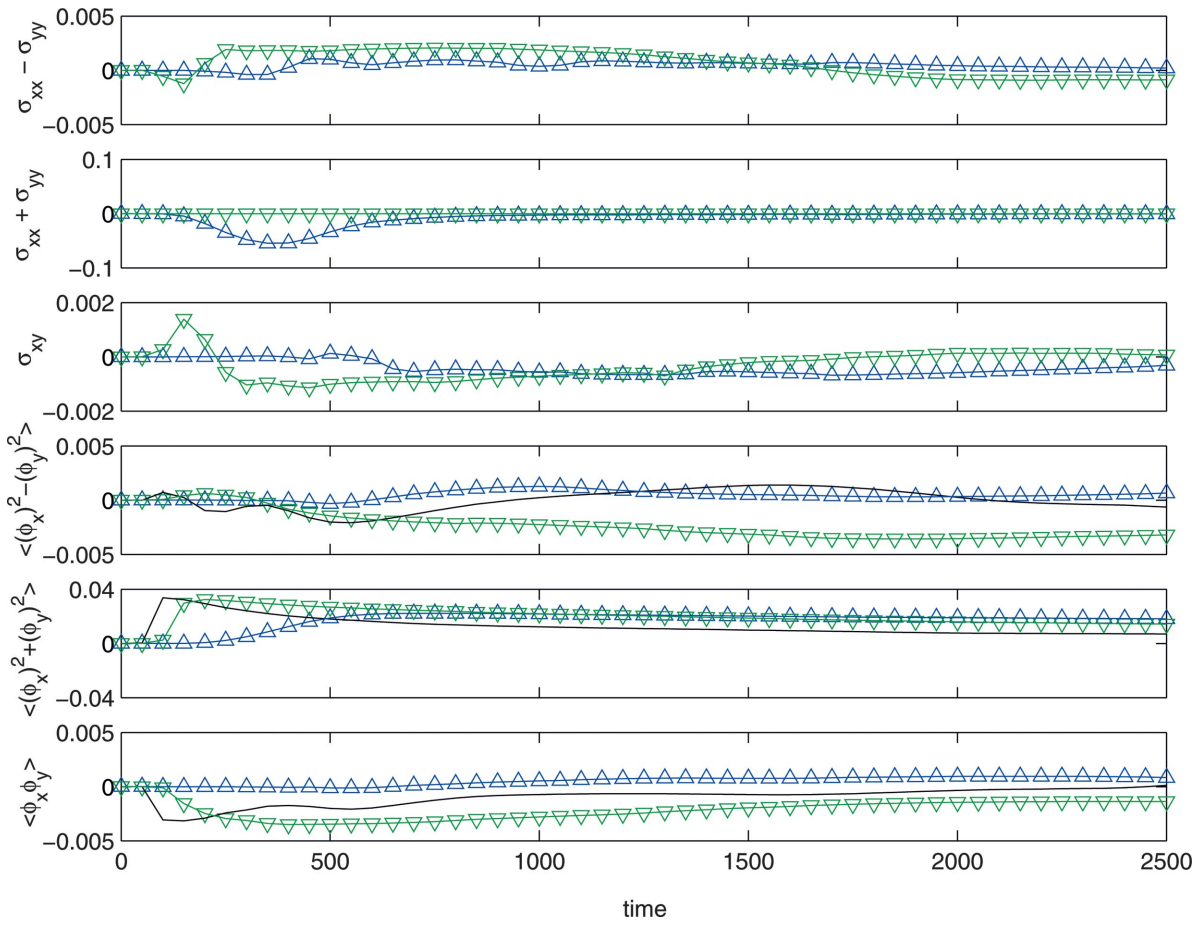


FIG. 2. (Color online) Top three panels: evolution of the normal, bulk, and shear stresses for the situation depicted in Fig. 1. The stresses are calculated by averaging the local stresses over the entire system. Bottom three panels: evolution of the interfacial stresses for the situation depicted in Fig. 1. The curve with triangles represents the full viscoelastic model; the inverted triangle (green) represents the viscoelastic model without bulk modulus. The solid line in the bottom three curves represents the nonviscoelastic purely hydrodynamic case.

$$\overleftrightarrow{M} = \begin{bmatrix} 2\dfrac{\partial v_{Ax}}{\partial x} & \left(\dfrac{\partial v_{Ax}}{\partial y} + \dfrac{\partial v_{Ay}}{\partial x}\right) \\ \left(\dfrac{\partial v_{Ax}}{\partial y} + \dfrac{\partial v_{Ay}}{\partial x}\right) & 2\dfrac{\partial v_{Ay}}{\partial y} \end{bmatrix}. \tag{8}$$

The velocity $\vec{v}_A$ represents the velocity of the viscoelastic phase defined as

$$\vec{v}_A = \vec{v} + \vec{v}_{applied} - \frac{(1-\phi)^2}{\zeta}[\vec{\nabla}\cdot\overleftrightarrow{\Pi} - \vec{\nabla}\cdot\overleftrightarrow{\sigma}]. \tag{9}$$

The above definition of $\overleftrightarrow{M}$ assumes that the stress acts on the viscoelastic fluid only. The final stresses $\overleftrightarrow{\sigma}_b^f$ and $\overleftrightarrow{\sigma}_s^f$ are given by $\overleftrightarrow{\sigma}_b^f = (1/2)Tr(\overleftrightarrow{\sigma}_b)\overleftrightarrow{I}$ and $\overleftrightarrow{\sigma}_s^f = \overleftrightarrow{\sigma}_s - (1/2)Tr(\overleftrightarrow{\sigma}_s)\overleftrightarrow{I}$. The total stress is given by $\overleftrightarrow{\sigma} = \overleftrightarrow{\sigma}_b^f + \overleftrightarrow{\sigma}_s^f$. The model described in Eqs. (1)–(9) can be used to simulate the viscoelastic phase separation under shear flow with shear rate $s$.

## III. VISCOELASTIC PHASE SEPARATION UNDER SHEAR FLOW

We describe our results on simulations of viscoelastic phase separation, both with and without shear. The model described in Sec. II is discretized on a $128\times128$ grid with periodic boundary conditions, using a spectral approach for the velocity equation and explicit, central difference schemes ($\Delta=1$, $\Delta t=0.005$) for the rest.

The applied velocity profile is symmetric about the ($x=x_0$) line. This allows periodic boundary conditions to be used during the application of shear. The effects of using such a profile are negligible in the long-time limit as the asymptotic morphologies are not influenced by the shear profile. A scheme that transforms coordinates [16,17] so that the regular shear profile is mapped to one involving periodic boundary conditions was also used. However, this leads to numerical instability and heterogeneities at long times for high shear rates. For the current viscoelastic model this scheme worked successfully until times of order $t=500$ for shear rates, $s=0.01$ and 0.1. The scheme was successfully tested with constant mobility in the order parameter equation for a purely hydrodynamic model [17] but led to numerical

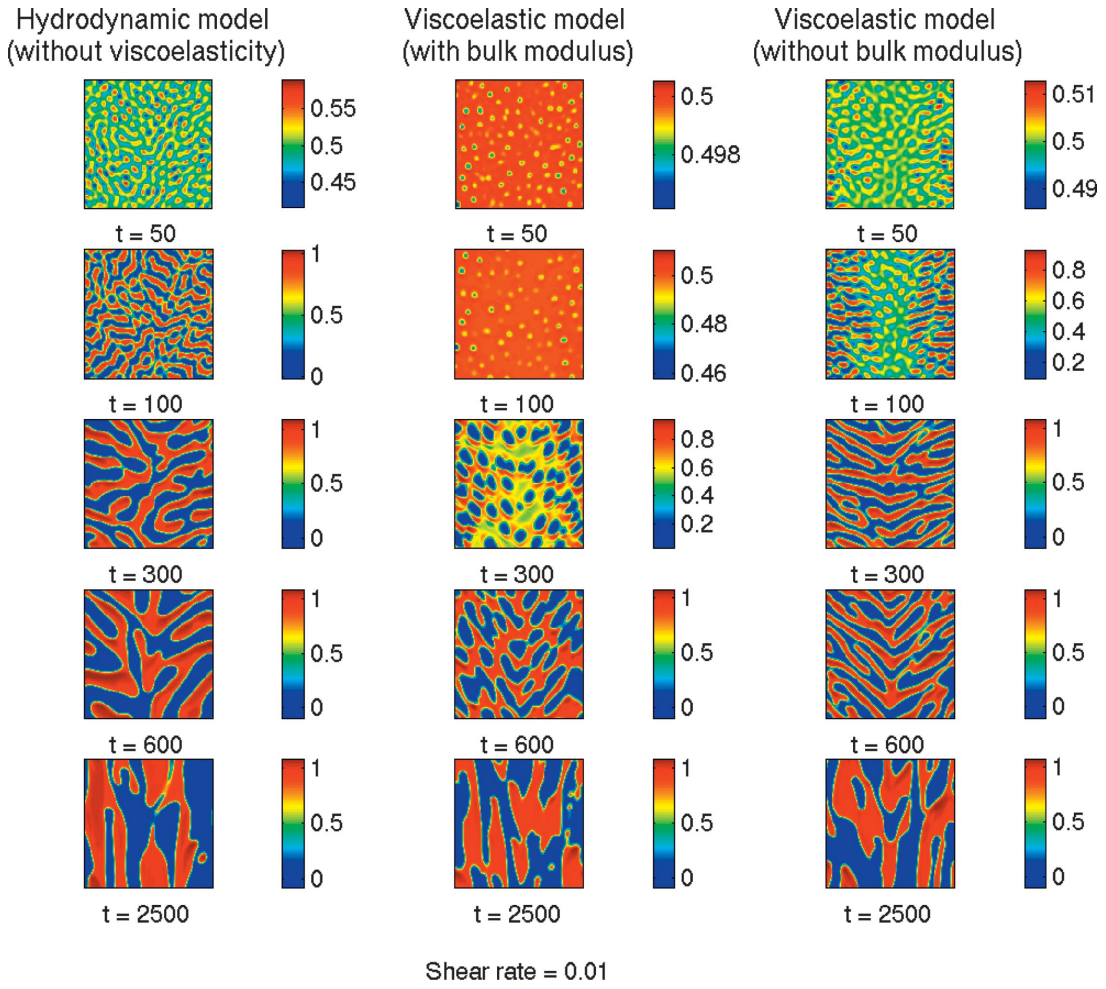


FIG. 3. (Color online) Phase separation process with shear flow of shear rate $s=0.01$ for the purely hydrodynamic case, the viscoelastic case with bulk modulus, and the viscoelastic case without bulk modulus. Shear is applied along the $y$ direction and periodic boundary conditions are assumed.

instabilities for the order-parameter-dependent mobility case discussed in the present work. Thus, for the sake of computational simplicity, we use the shear profile in Eq. (2).

Following Tanaka and Araki [8,9], we choose a step function $m_b=m_b^0\theta(\phi-\phi_0)$ ($\phi_0$ is the initial concentration before quenching), $m_s=m_s^0\phi^2$, $\tau_b=\tau_b^0\phi^2$, and $\tau_s=\tau_s^0\phi^2$. With this choice of moduli and time scales, Tanaka and Araki were able to reproduce a number of experimental features of viscoelastic phase separation [8,9].

We first simulate phase separation without an external shear ($s=0$). We consider a 50-50 mix with initial concentration fixed at $\phi_0=0.5$. The field $\phi(\vec{r},0)$ is initialized by small fluctuations of order 0.001 around $\phi_0$ and the model in Sec. II is simulated for three different cases. Case I corresponds to hydrodynamic phase separation in the absence of viscoelastic effects. Here we set all the stresses to zero and solve Eqs. (3) and (5) with only one velocity field $\vec{v}$. Case II is the full asymmetric viscoelastic model with $\eta_s=1$, $\zeta=0.1$, $m_b^0=5$, $m_s^0=0.5$, $\tau_b^0=10$, and $\tau_s^0=50$. To clarify the role of the bulk stress, in case III we switch off the bulk modulus—i.e., $m_b^0=0$.

Figure 1 shows the phase separation process for the three cases. The left column shows the nonviscoelastic (hydrodynamic) case, the middle column depicts the full viscoelastic model with asymmetric bulk modulus, and the right column represents the phase separation for the viscoelastic case without bulk modulus. This figure shows the importance of the bulk modulus in the formation of a network of the more viscoelastic component. For the case with the bulk modulus, initially, holes of the nonviscoelastic phase are formed in a partially phase-separated matrix of the more viscoelastic phase. As these holes grow, the area of the viscoelastic region decreases and a networklike structure is formed. These results are consistent with earlier results of Tanaka and Araki [8]. For the full viscoelastic model, we do not observe the breaking of the network within the time interval we simulated. The case without the bulk modulus appears to be similar to the purely hydrodynamic case and there is no network formation. Figure 1 also shows that viscoelastic effects slow down the domain growth, as can be inferred by comparing the domain patterns at time $t=1000$ for all three cases.

We have also monitored the evolution of the relevant stresses during the phase separation. The top three panels in

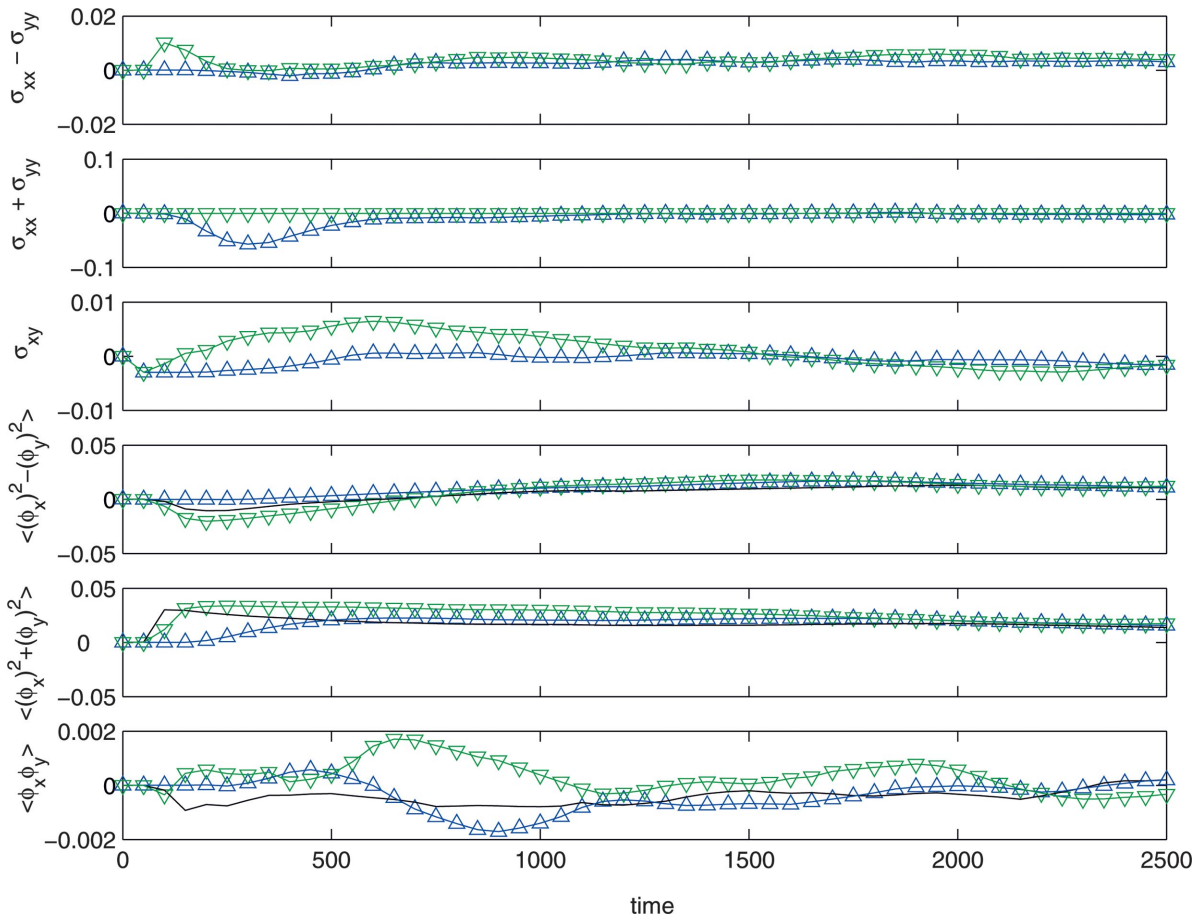


FIG. 4. (Color online) Top three panels: evolution of the normal, bulk, and shear stresses for the situation depicted in Fig. 3. Bottom three panels: evolution of the interfacial stresses for the situation depicted in Fig. 3. Meaning of symbols is same as Fig. 2.

Fig. 2 show the behavior of the average normal stress $\sigma_{xx}-\sigma_{yy}$, the average bulk stress $\sigma_{xx}+\sigma_{yy}$, and the average shear stress $\sigma_{xy}$ for the case with bulk stress as well as that for the case without bulk stress. The normal and shear stresses do not decay completely in the time simulated and exhibit small fluctuations of order 0.001, possibly due to the motion of the viscoelastic phase. The role of the bulk stress is similar to that for the case with nonzero bulk modulus; the early stage of phase separation is associated with significant compressive stresses. The compressive stresses are associated with the formation of the network of the more viscoelastic phase. The network of the partially phase-separated viscoelastic phase shrinks as the phase separation proceeds, resulting in the compressive stresses observed in the early stages. The interfaces also contribute to the stresses, and following Refs. [18,19], we define the normal interfacial stress as $\langle(\partial\phi/\partial x)^2-(\partial\phi/\partial y)^2\rangle$, the bulk interfacial stress as $\langle(\partial\phi/\partial x)^2+(\partial\phi/\partial y)^2\rangle$, and the shear interfacial stress as $\langle(\partial\phi/\partial x)(\partial\phi/\partial y)\rangle$. The bottom three panels in Fig. 2 show the evolution of the interfacial stresses for the situation depicted in Fig. 1. We also show the interfacial stresses for the nonviscoelastic case (solid lines in the bottom three panels). The fluctuations in these stresses are governed by the interfacial motion. Notice that the bulk interfacial stresses are higher compared to the normal and shear interfacial stresses. This is because the normal and shear interfacial stresses can locally take positive as well as negative values and, consequently, the average is small.

In Fig. 3, we display the phase separation process when an external shear with shear rate $s=0.01$ is applied. As in the case without shear, we consider three cases corresponding to the hydrodynamic case without viscoelastic effects, the full viscoelastic model with bulk modulus, and the viscoelastic model without bulk modulus. At this shear rate, the very early stages are not influenced significantly by the applied shear for all cases. At later times, there is an underlying tendency for the domains to align along the shear direction, although the alignment is not complete within the time simulated ($t=2500$). The case with the bulk modulus exhibits network morphologies in the earlier stages even for this case. The alignment is also slower in the initial stages for the case with the bulk modulus.

The time evolution of viscoelastic stresses for this value of shear is shown in Fig. 4 (top three panels) for the case with bulk stress as well as the case without bulk stress. Fluctuations due to random motion of domains in the early stages are observed for both normal and shear stresses and the amplitude of the fluctuations decreases at late times as the domains tend to align with the flow direction. For this case also, the bulk stress for the case with bulk modulus becomes

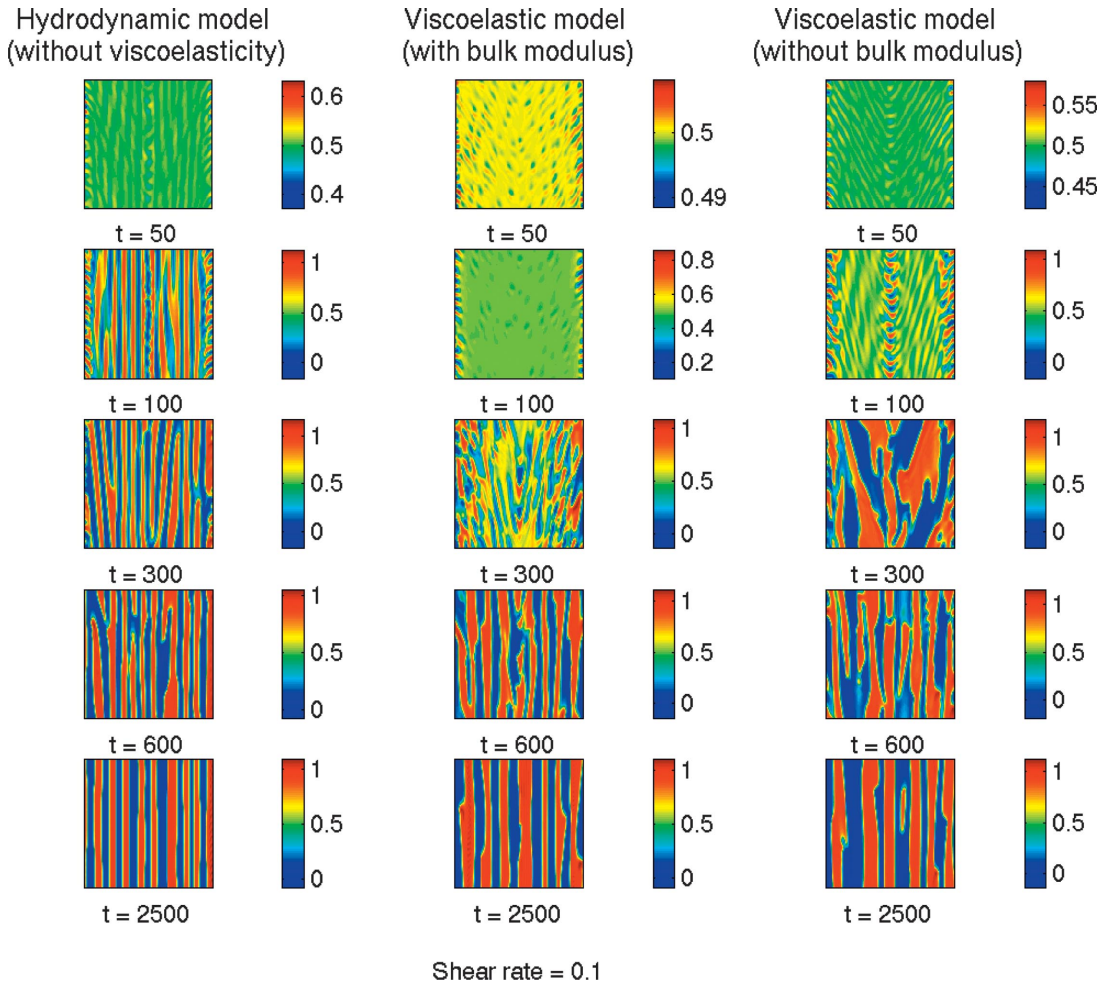


FIG. 5. (Color online) Phase separation process with shear flow of shear rate $s=0.1$ for the purely hydrodynamic case, the viscoelastic case with bulk modulus, and the viscoelastic case without bulk modulus. Shear is applied along the $y$ direction and periodic boundary conditions are assumed.

negative in the early stages, indicating the shrinking of the network of the viscoelastic phase. This alignment also influences the interfacial stresses, as can be seen in the bottom three panels in Fig. 4. The bulk and normal stresses for all cases approach a fixed value as at long times $\partial\phi/\partial y \rightarrow 0$ because of the alignment. Due to the decaying concentration gradient along the $y$ direction, the corresponding shear interfacial stresses are also small compared to the bulk and normal interfacial stresses.

Finally, we consider phase separation under a relatively large shear rate $s=0.1$. Figure 5 shows the phase separation at this shear rate for all three cases. For this case, the external shear effects dominate the phase separation and the tendency of the domains to align with the shear to form stringy patterns is much stronger than the earlier case. The purely hydrodynamic model rapidly forms the stringy phase, whereas for the viscoelastic cases, the intermediate stages are characterized by complex motion of the domains. For the case with the bulk modulus, the early stages do not show the formation of a well-developed network as the shear dominates over the internal dynamics. The snapshots at $t=2500$ show that a stringy phase seems to form at long times for the viscoelastic cases also, although the width of the lamellae is larger compared to the hydrodynamic case.

The top three panels of Fig. 6 show the time evolution of the viscoelastic stresses for this case. After transient fluctuations, the normal stresses decay to zero as the steady state is established. Compressive bulk stresses are observed even for this case but the magnitude is smaller for this case, compared to the earlier cases. This is due to the fact that the shear flow is so fast that the transient network of the viscoelastic phase is not able to fully develop. This is clear from the snapshot at time $t=50$ for the viscoelastic case. The behavior of the shear stresses is interesting. At long times, the shear stresses saturate to nonzero values. The saturation stresses are related to the effective shear viscosities for this binary fluid. The bottom three panels show the interfacial stresses. Since there is an almost perfect stringy phase formation in the long-time limit, the interfacial stresses attain their steady values. Notice that the bulk and normal stresses are almost the same due to

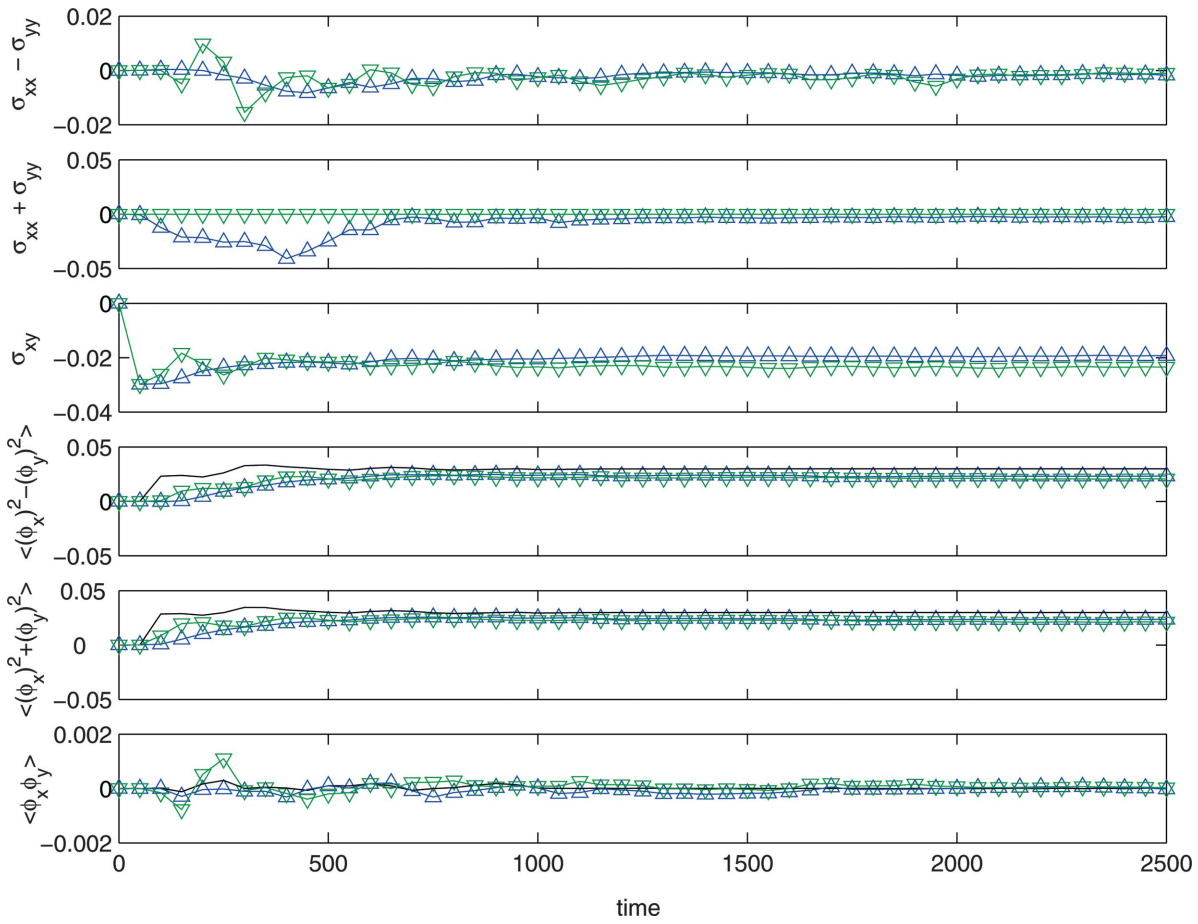


FIG. 6. (Color online) Top three panels: evolution of the normal, bulk, and shear stresses for the situation depicted in Fig. 5. Bottom three panels: evolution of the interfacial stresses for the situation depicted in Fig. 5. Meaning of the symbols is same as Fig. 2.

the vanishing concentration gradient in the $y$ direction. For the same reason, shear interfacial stresses also decay in the long-time limit.

## IV. PHASE-SEPARATED STABLE STATES UNDER SHEAR

So far we have considered the effects of shear on binary fluids undergoing phase separation. In this section we apply shear on stable phase-separated morphologies. The aim of this section is to explore the possibilities of using this model to study mechanical properties of polymer solutions and blends. Recently, Buxton and Balazs [14] have used a block and spring model to simulate the deformation of a random two-phase morphology obtained from a Cahn-Hilliard simulation. In this approach, there is no coupling between the morphologies and the deformation. Such an approach can only be used to study linear elastic behavior and does not describe the full viscoelastic response. The morphologies cannot evolve in response to deformation. However, the two-fluid framework used in this paper explicitly incorporates a coupling between the stress and the concentration and therefore it can describe deformation-induced morphological evolution.

We consider a simple phase-separated morphology below the coexistence temperature. We consider a 50-50 ($\phi_0=0.5$) binary fluid that exists as a band of fluid $A$ sandwiched between layers of fluid $B$. This is a stable phase-separated configuration. Polymer blends can show such macro phase separation in equilibrium and block copolymers also micro phase separate into lamellar morphologies [20]. We apply shear in the same way as discussed in the previous section. We consider two different shearing conditions. In one case the shear is normal to the $A/B$ interface, and in the other case the shear is parallel to the interface. Such a situation (for block copolymers) has been investigated experimentally [21] and theoretically using hydrodynamic models [22]. The morphological evolution for the case of shear normal to the $A/B$ interface is depicted in Fig. 7. All three cases that have been discussed in the previous section are simulated for this case also. For all the cases, initially the interface starts to move in response to the shear and at long times there is a tendency to form many bands aligned along the shearing direction. The bands appear to be wider for the viscoelastic cases in comparison to the hydrodynamic case. However, we do not find much difference between the case with bulk modulus and the case without bulk modulus. Interestingly, for the case when the shear is applied parallel to the interface, the band remains stable and no morphological evolution is observed for all three cases. This is consistent with the shear-induced reorientation

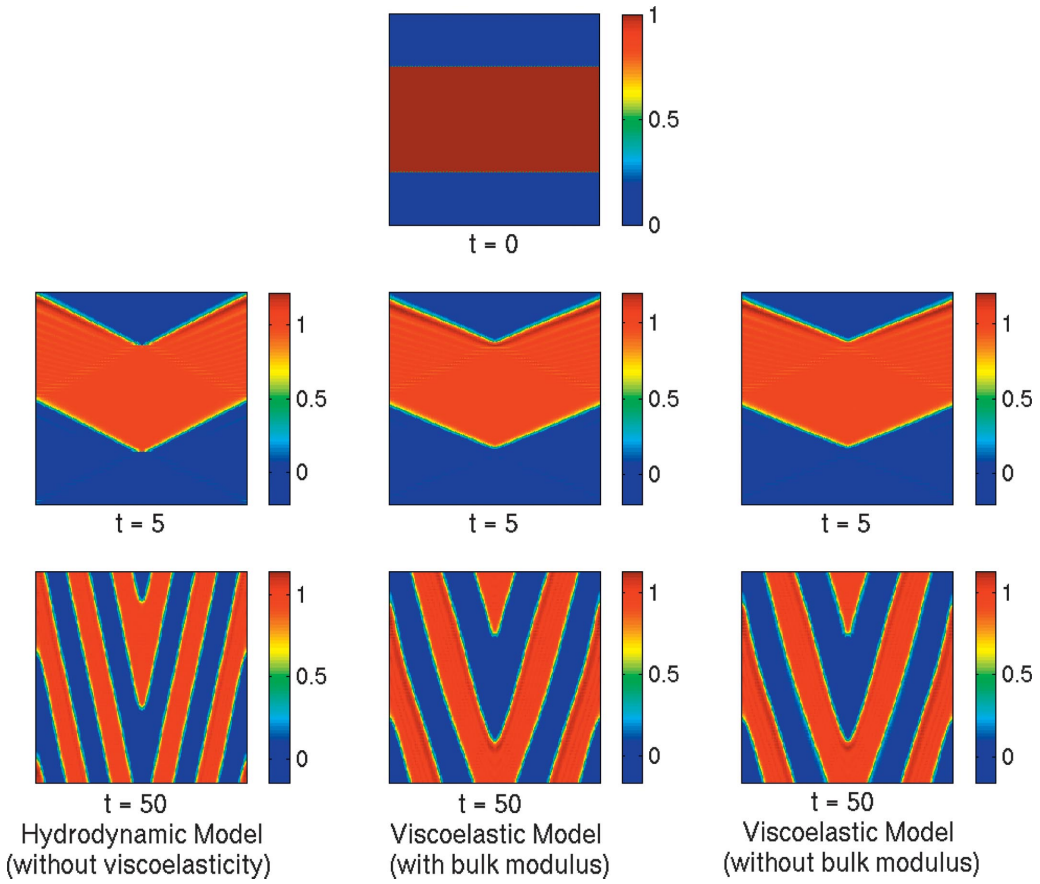


FIG. 7. (Color online) Evolution of the band morphology under a shear flow of shear rate $s=0.1$ for the purely hydrodynamic case, the viscoelastic case with bulk modulus, and the viscoelastic case without bulk modulus. Shear is applied along the $y$ direction and periodic boundary conditions are assumed.

of lamella for block copolymers observed in experiments [21] and theoretical models [22].

The three panels of Fig. 8 show the evolution of viscoelastic stresses for the full viscoelastic model (with bulk modulus) for both cases (shear parallel and perpendicular to the interface). For shear parallel to the interface, the normal and bulk stresses remain zero during the shearing process. This is because there are no morphological changes and only shear stresses are generated. For the case of shear perpendicular to the interface, normal as well as bulk stresses are generated due to shear-induced motion of the interface depicted in Fig. 7. For a short interval, weak compressive stresses are observed. The early-time behavior of the shear stress also differs from the case when the shear is applied parallel to the interface. This figure demonstrates the role played by morphological evolution on the viscoelastic properties of binary fluids. For the case without bulk modulus, very similar stress evolution (not shown here) is observed. However, no bulk stress is generated. The appropriate interfacial stresses are determined by the concentration gradients across the flat interfaces and are not shown as they do not exhibit particularly interesting behavior.

Finally, we study the relaxation of the morphologies after the applied shear is suddenly removed. We remove the shear at $t=50$ corresponding to the morphologies shown in the bottom row of Fig. 7. Figure 9 shows the final morphologies at $t=2150$ after removing the shear. It is clear that the morphological relaxation is much faster for the nonviscoelastic case and the band reappears, although it is shifted from the original position. For the viscoelastic cases, the morphological relaxation is very slow and the pattern does not return to the original band within the time span of the present simulations.

## V. SUMMARY

We have investigated the viscoelastic properties of dynamically asymmetric binary fluids under shear flow. The dynamical asymmetry arises as the binary fluid is constituted of one viscoelastic fluid and the other nonviscoelastic, purely hydrodynamic fluid. We have simulated phase separation for this binary fluid both with and without shear. Only for the case with a nonzero bulk modulus is there a tendency to form a network of the more viscoelastic phase in the initial stages of phase separation, both with and without shear flow. However, for the high shear rate, the network phase is short lived as the shear has a tendency to suppress network formation. For the high shear rate, in the long-time limit, a stringy phase is observed even for the viscoelastic cases; however, the length scales associated with the stringy phase are larger

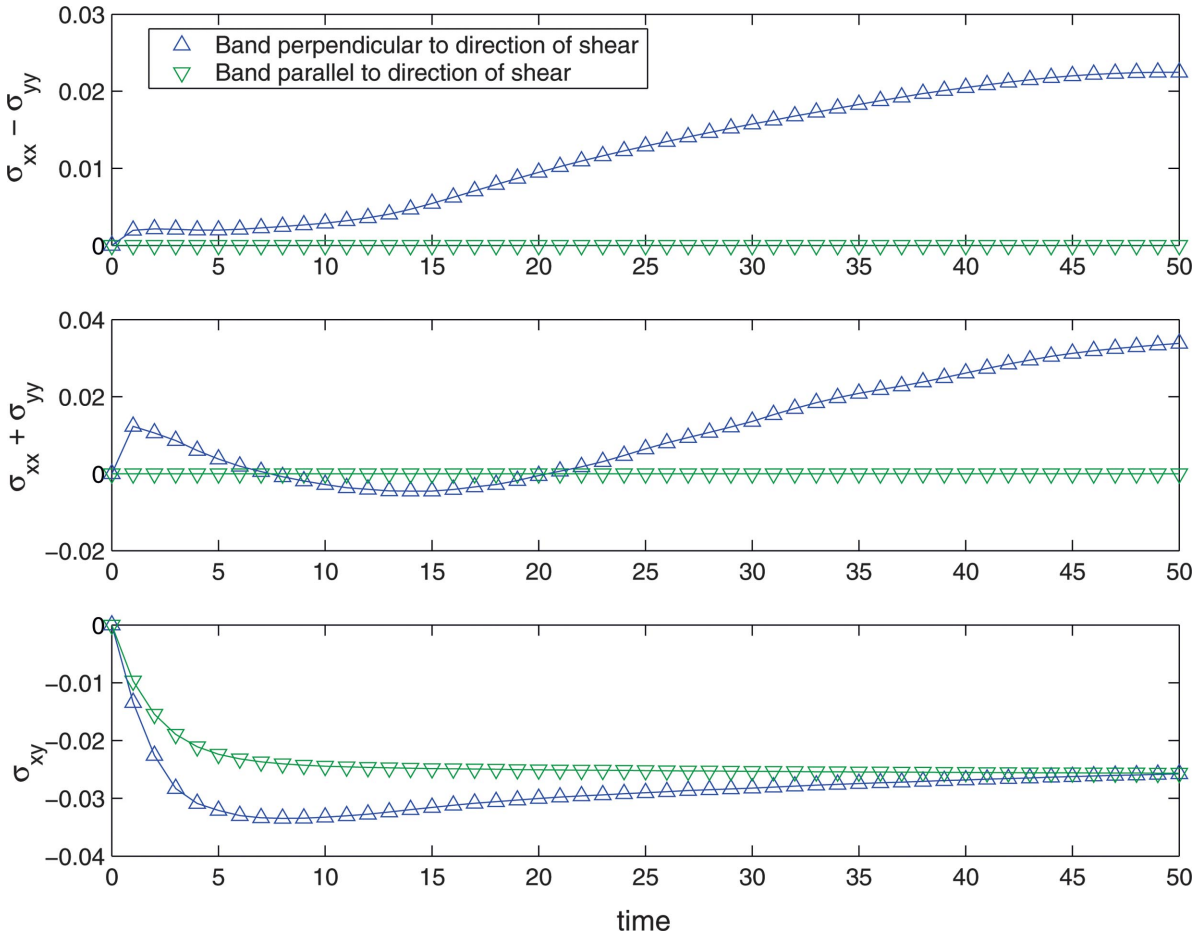


FIG. 8. (Color online) Evolution of the normal, bulk, and shear (mechanical) stresses for the case with nonzero bulk modulus (evolution depicted in the middle column of Fig. 7) for the two cases of shear parallel to the band and shear normal to the band.

compared to the purely hydrodynamic case. Thus, viscoelastic effects enhance the extent of phase separation under shear. We have also studied the temporal evolution of the effective viscoelastic stresses during the phase separation process. Interfacial motion results in fluctuations of the shear and normal stresses in the early stages. Transient compressive stresses are also observed corresponding to shrinking of viscoelastic phase in the early stages. At long times, the shear stresses saturate to a nonzero value. This value is related to the effective viscosity of the two-phase fluid.

We also investigated the effects of shear on stable phase-separated morphologies. A lamellar structure of the binary fluid below the coexistence temperature is sheared, both normal and parallel to the interface. There are crucial differences between these two cases. For shear parallel to the interface, no morphological evolution is observed, while for the case of shear normal to the interface, the interface moves and splits into bands that tend to align with the shear.

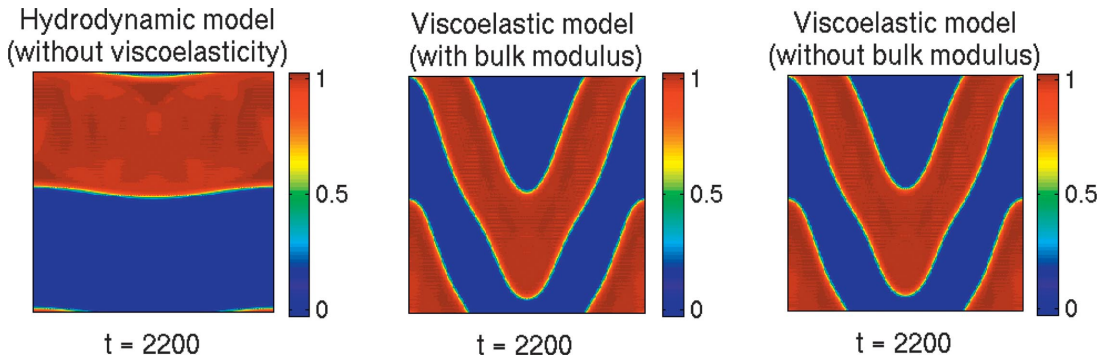


FIG. 9. (Color online) Morphologies for the three cases at $t=2150$ time steps after the shear flow has been removed. The shear flow was removed at $t=50$ steps after the shear was applied (corresponding to the bottom row in Fig. 7).

The evolution of effective stresses also depends on the direction of the interface. For example, for shear parallel to the interface, no bulk and normal stresses are generated. On the other hand, for shear normal to the interface, bulk, normal, and shear stresses are generated due to interfacial motion.

This paper demonstrates the role played by viscoelasticity on shearing of binary fluids. The simulations show that the underlying viscoelastic properties can significantly influence the shearing behavior. Further experiments are needed to test predictions of our simulations. The approach used in the present work can also be applied to other complex fluids such as block copolymers and microemulsions.

## ACKNOWLEDGMENTS

V.D. is grateful to the LANL-UCSB CARE program for providing support through a summer student stipend. This work was supported by the U.S. Department of Energy.

[1] H. Tanaka, Phys. Rev. Lett. **71**, 3158 (1993).
[2] H. Tanaka, Phys. Rev. Lett. **76**, 787 (1996).
[3] T. Hashimoto, K. Matsuzaka, E. Moses, and A. Onuki, Phys. Rev. Lett. **74**, 126 (1996).
[4] Y. Wu, H. Skrdla, and T. Lookman, Physica A **239**, 428 (1997).
[5] E. Helfand and G. H. Fredrickson, Phys. Rev. Lett. **62**, 2468 (1989).
[6] M. Doi and A. Onuki, J. Phys. II **2**, 1631 (1992).
[7] T. Taniguchi and A. Onuki, Phys. Rev. Lett. **77**, 4910 (1996).
[8] H. Tanaka and T. Araki, Phys. Rev. Lett. **78**, 4966 (1997).
[9] T. Araki and H. Tanaka, Macromolecules **34**, 1953 (2001).
[10] H. Tanaka, J. Phys.: Condens. Matter **12**, R207 (2000).
[11] J. N. Zhang, Z. L. Zhang, H. D. Zhang, and Y. L. Yang, Phys. Rev. E **64**, 051510 (2001).
[12] Y. L. Huo, H. D. Zhang, and Y. L. Yang, Macromolecules **36**, 5383 (2003).
[13] C. Sagui, L. Piche, A. Sahnoune, and M. Grant, Phys. Rev. E **58**, 4654 (1998).
[14] G. A. Buxton and A. C. Balazs, Interface Sci. **11**, 175 (2003).
[15] P. G. de Gennes, *Scaling Concepts in Polymer Physics*, 2nd ed. (Cornell University Press, Ithaca, NY, 1985).
[16] A. Onuki, J. Phys. Soc. Jpn. **66**, 1836 (1997).
[17] Z. Shou and A. Chakrabarti, Phys. Rev. E **61**, R2200 (2000).
[18] A. Onuki, Phys. Rev. A **35**, 5149 (1987).
[19] T. Ohta, H. Nozaki, and M. Doi, Phys. Lett. A **145**, 304 (1990).
[20] I. W. Hamley, *The Physics of Block Copolymers* (Oxford University Press, New York, 1998).
[21] A. Keller, E. Pedemonte, and F. M. Willmouth, Nature (London) **225**, 538 (1979).
[22] F. Drolet, P. Chen, and J. Viñals, Macromolecules **32**, 8603 (1999).